Discharge Characteristics of Multicell Lithium-Ion Battery with Nonuniform Cells

So Miyatake[a,1], Yoshihiko Susuki[a,*], Takashi Hikihara[a], Syuichi Itoh[b], Kenichi Tanaka[b]

[a] *Department of Electrical Engineering, Kyoto University*
Katsura, Nishikyo, Kyoto, 615-8510 Japan
[b] *CAPTEX Co., Ltd., 1-91, Shiinoki, Maigi-Cho, Okazaki, 444-3511 Japan*

Abstract

This paper addresses the discharge characteristics of a multicell lithium-ion battery with nonuniform cells. By using a multicell battery with two different types of cell, we experimentally investigate the relationship between discharge capacity and battery topology. In the series connection of nonuniform cells, the total capacity of the battery is governed by a cell with the smallest capacity. In the parallel connection, the total capacity becomes the sum of cells in parallel. In a multicell battery with the series-parallel connection, the discharge capacity depends on its configurations such as connection and number of nonuniform cells. Also, we derive a mathematical model for discharge characteristics of the multicell battery based on the equivalent circuit model of an individual cell. For a multicell battery with a general configuration, the discharge capacity is successfully evaluated by numerical simulations of the mathematical model.

Keywords:
Lithium-ion battery, Multicell battery, Discharge characteristics, Nonuniform cells, Battery topology, Modeling

*Corresponding author
Email address: susuki.yoshihiko.5c@kyoto-u.ac.jp (Yoshihiko Susuki)
[1] Presently, Nissan Motor Co., Ltd.

1. Introduction

Multicell lithium-ion battery is a system of energy storage that consists of multiple lithium-ion cells connected in series and parallel. Due to its high energy capacity, it is used in various applications such as electric vehicles and embedded systems [1, 2, 3, 4]. A multicell battery is initially synthesized using cells with a uniform characteristic [3, 4]. However, due to the repetitive charge / discharge operations, the initial uniformity of cell characteristics gradually breaks down. It is widely recognized that such nonuniform characteristics deteriorate the performance of the battery and cause a problem on safety and reliability [2, 4, 5]. In order to avoid the nonuniform characteristics, understanding the influence of nonuniform characteristics on the performance is of basic importance. This leads to design and management of high-confidence multicell batteries [6, 7, 8, 9].

Recently, researchers have focused on the discharge characteristics of multicell batteries with nonuniform cells. An effect of low-capacity cell on the battery performance was mentioned for the design of management systems [4]. A circuit-based model was derived to estimate the distribution of discharge currents in a general multicell battery [10, 11]. An iterative calculation-based method was also proposed for simulating discharge behaviors [12].

The purpose of this paper is to study the discharge characteristics of a multicell lithium-ion battery with nonuniform cells. As shown in [11], the discharge characteristics become complicated due to current effect, recovery effect, temperature effect, aging effect, and their interactions. To the best of our knowledge, no experimental analysis of the discharge characteristics in terms of nonuniform cells has been reported. Here, from a practical viewpoint, it is important to clarify the relationship between discharge characteristics and battery configurations such as connection and number of nonuniform cells. The multicell battery studied in this paper includes two different types of cell: one has large internal resistance and small capacity, and the other has small internal resistance and large capacity. By using a battery with one former cell and many latter cells, we experimentally investigate the relationship between discharge capacity and battery topology. The topology implies three distinguishable connections: series, parallel, and series-parallel connections. Also, we derive a mathematical model for evaluating the discharge capacity of a multicell battery. The effectiveness of the derived model is demonstrated with experiments and numerical simulations

of a battery with a general configuration.

The rest of this paper is organized as follows. Section 2 describes basic concepts of multicell battery. The experimental setup and procedure used in this paper are described in Section 3. Section 4 experimentally studies the discharge characteristics of a multicell battery in the series, parallel, and series-parallel connections. Section 5 analyzes a dependence of the battery configurations on the discharge capacity in the series-parallel connection by using experiments and numerical simulations. Section 6 is the conclusion of this paper with a brief summary and remarks.

2. Basic Concepts of Multicell Battery

Here, basic information about connections and characteristics of existing multicell batteries is introduced. There exist three distinguishable connections in a multicell battery, which we refer to as (i) series, (ii) parallel, and (iii) series-parallel connections [3, 4]. Series-parallel connection is further classified according to the existence of cross coupling: see Section 4.3 and Fig. 6. In this paper, N_{S} denotes the integer number of cells connected in series and N_{P} the integer number of cells in parallel. Also, $(N_{\mathrm{S}}, N_{\mathrm{P}})$ denotes the combination of number of cells in series and in parallel. A commercial multicell battery possesses a mixture of the three connections. From graph theory [13], every series-parallel network is aggregated as either series or parallel network. This suggests that arbitrary connection is aggregated as either basic series connection or parallel connection [11, 12]. On the basis of this fact, in this paper we define the basic series and parallel connections as $(N_{\mathrm{S}}, N_{\mathrm{P}}) = (2, 1)$ and $(N_{\mathrm{S}}, N_{\mathrm{P}}) = (1, 2)$. Also, a multicell battery is generally synthesized using cells with a uniform characteristic. In this uniform case, the discharge characteristics on the series-parallel connection are explained in terms of the basic series and parallel connections [11, 12]. On the other hand, in the case of nonuniform cells, no explanation has been reported in terms of basic connections.

3. Experimental System and Procedure

This paper studies the multicell battery in which only one cell is different from the others. In Section 4, based on the idea of aggregation mentioned above, we experimentally analyze the discharge characteristics of the series and parallel connections with two cells shown in Fig. 1. Then, the discharge

characteristics are analyzed in the case of series-parallel connection denoted as $(N_{\mathrm{S}}, N_{\mathrm{P}}) = (2, 2)$.

The experimental system and procedure used in this paper are described below. Fig. 2 shows the overview of the experimental system. In order to uniform the initial conditions, individual cells were first charged to their full capacities under the conditions of constant current and constant voltage. Every cell was charged until its open-circuit voltage reached $4.15\,\mathrm{V}\pm10\,\mathrm{mV}$. Then, the multicell battery with the full-charged cells was connected to the electronic load (TEXIO, LW151-151D) and was discharged until the terminal voltage of a cell reached its cut-off voltage of $2.5\,\mathrm{V}\pm10\,\mathrm{mV}$. During the discharge operation, the electronic load was operated under the constant resistance at $4.8\,\Omega$ per a cell. The terminal voltage and current of every cell were measured and recorded using the data loggers (KEYENCE, NR-500). The current was measured with the current sensing resistors at $5\,\mathrm{m}\Omega$ (Welwyn Components, OAR-3). Then, the discharge capacity was calculated by numerically integrating the measured current during the period of discharge operation. All experiments in this paper were conducted at room temperature. Ambient temperature for the experiments is presented in each caption of figures.

Two types of cylindrical cells, which were ICR (BYD, ICR18650) and NCR (Panasonic, NCR18650), were used in the experiments. The ICR cell was used as the one different cell. The rated characteristics of ICR and NCR are summarized in Tab. 1. The nominal discharge capacity of ICR is 2350 mAh and is smaller than the nominal capacity (2900 mAh) of NCR. Fig. 3 shows the measured discharge voltage and internal resistance for ICR and NCR. The internal resistance was measured using the i-R drop between terminal voltage and open-circuit voltage [3]. In Fig. 3, the terminal voltage of ICR is lower than NCR, because of the large internal resistance and the low open-circuit voltage of ICR.

4. Experiments

This section experimentally investigates the discharge characteristics in the basic connections of nonuniform cells. Here, the discharge characteristics in the series-parallel connection are evaluated in terms of the basic series and parallel connections. In this paper, A + B denotes the series connection of cells A and B, and A $\|$ B the parallel connection of cells A and B, respectively.

Also, $Q_{\mathrm{S}}(\mathrm{A})$ denotes the discharge capacity of cell A in the case of a single operation.

4.1. Series Connection

First, we experimentally investigate the discharge characteristics of two cells in series. As shown in Fig. 1(a), one ICR (I1, 2326 mAh) and one NCR (N1, 2839 mAh) were connected in series and discharged to a load of $9.6\,\Omega$ ($= 4.8\,\Omega \times 2$). Tab. 2 summarizes the measured discharge capacity, and Fig. 4 shows the measured discharge voltage and current of each cell. Discharge capacity, voltage, and current are also shown in the case of a single operation. In the series connection, the current of each cell is common as shown in Fig. 4(b). As a result, the terminal voltage of I1 reaches its cut-off voltage earlier than N1: see Fig. 4(a). Here, the discharge capacity of the battery is 2303 mAh and is close to $Q_{\mathrm{S}}(\mathrm{I1})$. In this case, N1 has nonzero amount of charge that corresponds to $Q_{\mathrm{S}}(\mathrm{N1}) - Q_{\mathrm{S}}(\mathrm{I1})$ at the end of discharge operation. Thus, the total capacity of the battery is determined by the cell with the small capacity in the series connection.

4.2. Parallel Connection

Next, the discharge characteristics of two cells in parallel are experimentally investigated. I1 and another NCR, denoted as N2 with 2820 mAh, were connected in parallel and discharged to a load of $2.4\,\Omega$ ($= 4.8\,\Omega/2$). The results are shown in Tab. 3 and Fig. 5. In contrast to the series connection, the terminal voltage of each cell is common as shown in Fig. 5(a). During the discharge operation, each cell discharges from an initial voltage to its cut-off voltage. As a result, the discharge capacities of I1 and N2 almost correspond to $Q_{\mathrm{S}}(\mathrm{I1})$ and $Q_{\mathrm{S}}(\mathrm{N2})$, respectively: see Tab. 3. Thus, in the parallel connection of two cells with nonuniform characteristics, the total capacity of the battery becomes the sum of individual cells. In this connection, the discharge current of the battery is not equally distributed to each cell as shown in Fig. 5(b).

4.3. Series-Parallel Connection

Here, the discharge characteristics in the series-parallel connection are investigated. The connections of four cells are shown in Fig. 6. As mentioned in Section 2, the connections are distinguished according to the existence of cross coupling. I1 and three NCR cells (N1, N2, N3) were connected and discharged to a load of $4.8\,\Omega$.

4.3.1. With Cross Coupling

First, we present the experimental results for multicell battery with cross coupling. Tab. 4 summarizes the measured discharge capacity and Fig. 7 shows the measured discharge voltage and current of each cell. In Tab. 4, the discharge capacities of I1 and N2 correspond to $Q_{\mathrm{S}}(\mathrm{I1})$ and $Q_{\mathrm{S}}(\mathrm{N2})$, respectively. The discharge capacities of N1 and N3 are around 2550 mAh. The capacities are smaller than $Q_{\mathrm{S}}(\mathrm{N1})$ $(= Q_{\mathrm{S}}(\mathrm{N3}))$ and almost half of the sum $Q_{\mathrm{S}}(\mathrm{I1}) + Q_{\mathrm{S}}(\mathrm{N2})$. The total discharge capacity of the battery is 5121 mAh. These results imply that the total discharge capacity is restricted by I1 $\parallel$ N2. This is consistent with the results on the series connection in Section 4.1. The connection of cells in Fig. 6(a) is aggregated as the series connection of I1 $\parallel$ N2 and N1 $\parallel$ N3. From the results on the series connection, the discharge capacity of the battery is restricted by I1 $\parallel$ N2. Then, from the results on the parallel connection, the discharge capacity is calculated as the sum $Q_{\mathrm{S}}(\mathrm{I1}) + Q_{\mathrm{S}}(\mathrm{N2})$. The sum is almost equal to the experimentally estimated capacity. The distribution of currents in I1 and N2 on Fig. 7(b) is almost the same as in the case of the parallel connection of I1 and N2 in Fig. 5(b). Thus, the discharge characteristics of the battery with cross coupling are evaluated in terms of the basic connections.

4.3.2. Without Cross Coupling

Next, the experimental results on the case of no cross coupling are presented in Tab. 5 and Fig. 8. In Fig. 8(a), when I1 reaches its cut-off voltage, the discharge capacity of I1 becomes 2314 mAh and corresponds to $Q_{\mathrm{S}}(\mathrm{I1})$. Then, the discharge capacity of N1 is restricted by I1 and becomes 2303 mAh. The discharge capacities of N2 and N3 are around 2700 mAh and smaller than $Q_{\mathrm{S}}(\mathrm{N2})(= Q_{\mathrm{S}}(\mathrm{N3}))$. The total discharge capacity of the battery is 5009 mAh.

By the same manner as the cross coupling, the series-parallel connection in Fig. 6(b) is aggregated as the parallel connection of I1 + N1 and N2 + N3. However, any combination of the results on the basic series and parallel connections does not lead to the experimentally estimated capacity. Here, the sum of terminal voltages of cells connected in series is common for each string of cells. Therefore, the terminal voltages of the uniform cells N2 and N3 are determined by the number N_{S} of cells in series and correspond to the half of the total voltage in the experiment. The terminal voltage of N2 (or N3) does not reach its cut-off voltage, while the terminal voltage of I1 reaches its cut-off voltage. In this way, the discharge capacity of N2 (or N3) does not reach $Q_{\mathrm{S}}(\mathrm{N2})$ (or $Q_{\mathrm{S}}(\mathrm{N3})$). Since the evaluation in the basic series

connection is based on the discharge capacity of a single operation, it does not explain the experimental result in the case of no cross coupling. This conclusion suggests that the discharge capacity of the battery depends on its configuration and the terminal voltage of every cell.

5. Numerical Simulations

This section describes a mathematical model for the evaluation of discharge capacity in the series-parallel connection. Here we investigate a dependence of the battery configurations on the discharge capacity of the general multicell battery in Fig. 9. The battery is synthesized with one ICR cell and many NCR cells.

5.1. Mathematical Model

In Section 4.3.2, it is experimentally observed that the terminal voltage of each cell governs the discharge capacity of the battery. Based on the experimental observation, we can adopt the circuit-based cell model reported in [14, 15] for analysis of the multicell battery. The cell model consists of a controlled voltage source and a constant resistance, denoted as r. The open-circuit voltage $e(t)$ and terminal voltage $v(t)$ are represented by the following equations:

$$e(t) = E_0 - \frac{KQ_0}{Q_0 - \int_0^t i(\tau)\mathrm{d}\tau} + A\exp\left(-B\int_0^t i(\tau)\mathrm{d}\tau\right), \tag{1}$$

$$v(t) = e(t) - ri(t), \tag{2}$$

where E_0 is the initial voltage, K the voltage drop caused by polarization, Q_0 the initial capacity, and $i(t)$ the discharge current. The constants A and B are responsible for the initial voltage drop. The parameters for ICR and NCR are presented in Tab. 6. They were obtained by the method of least squares based on the experimental results on discharge characteristics at constant currents. Here, by defining the charge variable $q(t) := \int_0^t i(\tau)\mathrm{d}\tau$, the circuit-based cell model is re-written as

$$\left.\begin{aligned} e(q) &= E_0 - \frac{KQ_0}{Q_0 - q} + A\exp(-Bq), \\ \frac{\mathrm{d}q}{\mathrm{d}t} &= \frac{e(q) - v(t)}{r}. \end{aligned}\right\} \tag{3}$$

The variable $q(t)$ provides the discharge capacity by taking t as a final time of the operation, and thus the above circuit-based model is based on the observation in which the terminal and open-circuit voltages of a cell govern its discharge capacity.

For the current modeling, we use the following two properties based on the experimental results.

- P1 The current of a battery is equally distributed to every parallel connection with uniform cells.
- P2 The terminal voltage of every cell is common in any series connection with uniform cells.

In the experimental results on the series-parallel connection with cross coupling, the current of the battery is equally distributed to uniform cells N1 and N3 as shown in Fig. 7(b). On the other hand, in the series-parallel connection without cross coupling, the terminal voltages of uniform cells N2 and N3 are common as in Fig. 8(a). These properties are general because they are based on the standard Kirchhoff's laws for an electric circuit with identical cells.

With the circuit-based cell model and the above two properties, we derive a mathematical model for discharge characteristics of the multicell battery in Fig. 9. Now, all cells in the battery are classified into three types of cell A, B, and C as shown in Fig. 10. The classification is based on the behavior of terminal voltage of cells. Because the current of every cell is common in series connection and the sum of terminal voltages is common in the parallel connection, the relationship between terminal voltages for each string is described as

$$e_{\mathrm{A}} - i_1 r_{\mathrm{A}} + (N_{\mathrm{S}} - 1)(e_{\mathrm{B}} - i_1 r_{\mathrm{B}}) - N_{\mathrm{S}}(e_{\mathrm{C}} - i_2 r_{\mathrm{C}}) = 0, \tag{4}$$

where e_{A}, e_{B}, and e_{C} are the open-circuit voltage of cell A, B, and C. Also, r_{A}, r_{B}, and r_{C} are the internal resistance. The variable i_1 is the current of cell A and B, while i_2 is the current of cell C. By considering the load with a constant resistance R_{L}, the following equations are obtained:

$$i_1 + (N_{\mathrm{P}} - 1) i_2 = i_{\mathrm{L}}, \tag{5}$$

$$N_{\mathrm{S}}(e_{\mathrm{C}} - i_2 r_{\mathrm{C}}) - i_{\mathrm{L}} R_{\mathrm{L}} = 0, \tag{6}$$

where i_{L} is the load current. The matrix formulation of Eqs. (4), (5), and (6) is given as

$$\begin{bmatrix} 1 & N_{\mathrm{S}}-1 & -N_{\mathrm{S}} & -r_{\mathrm{A}}-(N_{\mathrm{S}}-1)r_{\mathrm{B}} & N_{\mathrm{S}}r_{\mathrm{C}} & 0 \\ 0 & 0 & 0 & 1 & N_{\mathrm{P}}-1 & -1 \\ 0 & 0 & N_{\mathrm{S}} & 0 & -N_{\mathrm{S}}r_{\mathrm{C}} & -R_{\mathrm{L}} \end{bmatrix} \begin{bmatrix} e_{\mathrm{A}} \\ e_{\mathrm{B}} \\ e_{\mathrm{C}} \\ i_1 \\ i_2 \\ i_{\mathrm{L}} \end{bmatrix} = \begin{bmatrix} 0 \\ 0 \\ 0 \end{bmatrix}. \tag{7}$$

In a normal setting, the above coefficient matrix, denoted as $\mathsf{M} = [\mathsf{M}_1\ \mathsf{M}_2]$ where $\mathsf{M}_i \in \mathbb{R}^{3\times 3}$, is column full-rank, and the sub matrix M_2 is regular. From these, the following linear relation of discharge currents and open-circuit voltages is obtained:

$$\begin{bmatrix} i_1 \\ i_2 \\ i_{\mathrm{L}} \end{bmatrix} = -\mathsf{M}_2^{-1}\mathsf{M}_1 \begin{bmatrix} e_{\mathrm{A}} \\ e_{\mathrm{B}} \\ e_{\mathrm{C}} \end{bmatrix} =: \begin{bmatrix} G_{11} & G_{12} & G_{13} \\ G_{21} & G_{22} & G_{23} \\ G_{31} & G_{32} & G_{33} \end{bmatrix} \begin{bmatrix} e_{\mathrm{A}} \\ e_{\mathrm{B}} \\ e_{\mathrm{C}} \end{bmatrix}, \tag{8}$$

The elements G_{ij} of the above matrix are presented in Appendix. Now, based on Eq. (8), the three models for the single cells A, B, and C are combined. With the two charge variables q_1 and q_2 defined as $\int_0^t i_j(\tau)\mathrm{d}\tau$ $(j = 1, 2)$, the models are given as

$$e_{\mathrm{A}}(q_1) = E_{0,\mathrm{ICR}} - \frac{K_{\mathrm{ICR}}Q_{0,\mathrm{ICR}}}{Q_{0,\mathrm{ICR}} - q_1} + A_{\mathrm{ICR}}\exp\left(-B_{\mathrm{ICR}}q_1\right), \tag{9}$$

$$e_{\mathrm{B}}(q_1) = E_{0,\mathrm{NCR}} - \frac{K_{\mathrm{NCR}}Q_{0,\mathrm{NCR}}}{Q_{0,\mathrm{NCR}} - q_1} + A_{\mathrm{NCR}}\exp\left(-B_{\mathrm{NCR}}q_1\right), \tag{10}$$

$$e_{\mathrm{C}}(q_2) = E_{0,\mathrm{NCR}} - \frac{K_{\mathrm{NCR}}Q_{0,\mathrm{NCR}}}{Q_{0,\mathrm{NCR}} - q_2} + A_{\mathrm{NCR}}\exp\left(-B_{\mathrm{NCR}}q_2\right), \tag{11}$$

where the suffix ICR (or NCR) represents the parameters for the single cell ICR (or NCR). Since each current variable is represented as a superposition of the three voltage variables (see Eq. (8)), the following set of differential equations with the two independent variables q_1 and q_2 is obtained:

$$\left.\begin{aligned} \frac{\mathrm{d}q_1}{\mathrm{d}t} &= G_{11}e_{\mathrm{A}}(q_1) + G_{12}e_{\mathrm{B}}(q_1) + G_{13}e_{\mathrm{C}}(q_2), \\ \frac{\mathrm{d}q_2}{\mathrm{d}t} &= G_{21}e_{\mathrm{A}}(q_1) + G_{22}e_{\mathrm{B}}(q_1) + G_{23}e_{\mathrm{C}}(q_2). \end{aligned}\right\} \tag{12}$$

These equations describe the dynamics of the charges for the three cells A, B, and C in a self-consistent manner and are hence used as a mathematical model for discharge dynamics of the multicell battery.

5.2. Verification

Here, the derived model for the multicell battery is verified in comparison with experiments on discharge capacity of the multicell battery. All experiments were performed on the battery with one ICR cell and eleven NCR cells. The discharge capacity of NCR was 2817 mAh in average, denoted as $Q_{\max}$, and was larger than the capacity of ICR, 2133 mAh, denoted as $Q_{\min}$. The battery was configured as $(N_{\mathrm{S}}, N_{\mathrm{P}})$ cells in series-parallel with the conditions $2 \leqq N_{\mathrm{S}} \leqq 6$, $2 \leqq N_{\mathrm{P}} \leqq 6$, and $N_{\mathrm{S}} \cdot N_{\mathrm{P}} \leqq 12$.

For comparison, we calculated the discharge capacity Q of a cell in the series connection with uniform NCR cells. The total capacity of the multicell battery possibly depends on the number of cells, and the estimated capacity Q becomes a quantitative measure of the $(N_{\mathrm{S}}, N_{\mathrm{P}})$ dependence of the discharge capacity. The quantity Q is simply calculated by the following equation:

$$Q = \int_0^T i_2(t)\mathrm{d}t, \tag{13}$$

where T is the final time of discharge operations. Fig. 11 shows the results on experiments and numerical simulations of the discharge capacity Q with $(N_{\mathrm{S}}, N_{\mathrm{P}})$ cells. The results clearly indicate that the discharge capacity Q depends on the number of cells. In Fig. 11, although the experimental results are slightly affected by the effect of cycle life and a slightly nonuniform characteristic in the NCR cells, the numerical and experimental results are almost consistent. The derived model accounts for the experimental data on discharge capacity in the multicell battery with nonuniform cells. In this model, the open-circuit voltage of an individual cell depends on the amount of discharge as well as discharge capacity. Therefore, the results in Fig. 11 confirm that the discharge capacity of a multicell battery is dominantly determined by the open-circuit voltages of individual cells.

In the experimental results, the minimum value of Q is 2416 mAh and the maximum value is 2700 mAh. In the simulations, the minimum value of Q is 2409 mAh and the maximum value is 2701 mAh. In every combination of N_{S} and N_{P}, Q exists in the range of $Q_{\min} < Q < Q_{\max}$. The capacity Q depends dominantly on N_{S} not on N_{P}. Also, Q decreases as N_{S} increases. The result

on the discharge capacity $Q < Q_{\max}$ implies that the multicell battery does not discharge the full of its charge. As the increase of N_{S}, this salient feature appears clearly and the multicell battery exhibits a small Q as shown in Fig. 11. For a sufficiently large N_{S}, from Eq. (4) the effect of the ICR cell A on the battery is negligible, and the battery is regarded as the two NCR cells B and C in parallel. Because B and C have the same characteristics, they will behave in a common manner at this extreme situation. Here, from the experimental result in Section 4.1, the discharge capacity of the string containing A is determined by a cell with the smallest capacity, that is, A with $Q_{\min}$. This is why as the increase of N_{S}, the value of Q decreases and approaches to $Q_{\min}$. On the other hand, the result on $Q > Q_{\min}$ implies that the discharge capacity of a multicell battery is not necessarily restricted by a cell with the smallest capacity. As discussed above, for the infinite N_{S} of cells, the single ICR cell governs the performance of the battery. On the other hand, in a finite N_{S}, the effect of the ICR cell is possibly weakened by the other uniform NCR cells. Thus, we show such a finite-number effect governs the performance of the battery with nonuniform cells. From the experimental result in Section 4.3.2, the finite-number effect is partly captured by the terminal or open-circuit voltage of every cell. The model derived in this section is based on the open-circuit voltage and is therefore successful for reproducing the finite-number effect observed in the experimental results of Fig. 11.

6. Concluding Remarks

This paper investigated the discharge characteristics of a multicell battery with nonuniform cells. The analysis reported in this paper reveals the relationship between discharge capacity and topology of the multicell battery. In the series connection of nonuniform cells, the total capacity of the battery is governed by a cell with the smallest capacity. In the parallel connection, the total capacity becomes the sum of individual cells in parallel. In the series-parallel connection of nonuniform cells, the discharge capacity depends on the configurations of the battery. For a multicell battery with a general configuration, the evaluation of discharge capacity is enabled by numerical simulations of the mathematical model which is newly derived in this paper.

Here we provide several remarks related to generalization of the experimental results described above. The experimental results on the series and

parallel connections are obtained for the multicell battery which consists of less than two cells. In the case of multiple cells in the series connection, the current of every cell is common in the same manner as the two cells. In the parallel connection of multiple cells, the terminal voltage of every cell is common. Therefore, the discharge characteristics on the series and parallel connections are valid in a multicell battery with more than two cells. The results obtained in this paper lead to a method for evaluating discharge characteristics of multicell batteries with arbitrary configurations.

Acknowledgments

The work was partially supported by NICT Research Project ICE-IT. We would like to thank Associate Professor Nobuo Satoh, Department of Electrical, Electronics and Computer Engineering, Chiba Institute of Technology, for his important preparation to the experimental setup and insightful discussion of the results.

References

[1] B. Scrosati, J. Garche, Lithium batteries: Status, prospects and future, Journal of Power Sources 195 (9) (2010) 2419–2430.

[2] H. J. Bergveld, W. S. Kruijt, P. H. L. Notten, Battery Management Systems Design by Modelling, Kluwer Academic Publishers, 2002.

[3] H. Horie, Lithium-ion Battery —Foundation and Application—, Baifukan Co., Ltd., 2010 (in Japanese).

[4] D. Andrea, Battery Management Systems for Large Lithium-Ion Battery Packs, ARTECH HOUSE, 2010.

[5] G. J. Offer, V. Yufit, D. A. Howey, B. Wu, N. P. Brandon, Module design and fault diagnosis in electric vehicle batteries, Journal of Power Sources 206 (2012) 383–392.

[6] V. Sukumar, M. Alahmad, K. Buck, H. Hess, H. Li, D. Cox, F. N. Zghoul, J. Jackson, S. Terry, B. Blalock, M. M. Mojarradi, W. C. West, J. F. Whitacre, Switch array system for thin film lithium microbatteries, Journal of Power Sources 136 (2) (2004) 401–407.

[7] M. Alahmad, H. Hess, M. Mojarradi, W. West, J. Whitacre, Battery switch array system with application for JPL's rechargeable micro-scale batteries, Journal of Power Sources 177 (2) (2008) 566–578.

[8] H. Kim, K. G. Shin, DESA: Dependable, Efficient, Scalable Architecture for Management of Large-Scale Batteries, IEEE Transactions on Indusrial Informatics 8 (2) (2012) 406–417.

[9] T. Kim, W. Qiao, L. Qu, Power Electronics-Enabled Self-X Multicell Batteries: A Design Toward Smart Batteries, IEEE Transactions on Power Electronics 27 (11) (2012) 4723–4733.

[10] J. Zhang, S. Ci, H. Sharif, M. Alahmad, An Enhanced Circuit-Based Model for Single-Cell Battery, in: Applied Power Electronics Conference and Exposition, 2010, pp. 672–675.

[11] J. Zhang, S. Ci, H. Sharif, M. Alahmad, Modeling Discharge Behavior of Multicell Battery, IEEE Transactions on Energy Conversion 25 (4) (2010) 1133–1141.

[12] M.-S. Wu, C.-Y. Lin, Y.-Y. Wang, C.-C. Wan, C. R. Yang, Numerical simulation for the discharge behaviors of batteries in series and/or parallel-connected battery pack, Electrochimica Acta 52 (3) (2006) 1349–1357.

[13] R. J. Duffin, Topology of Series-Parallel Networks, Journal of Mathematical Analysis and Applications 10 (1965) 303–318.

[14] O. Tremblay, L.-A. Dessaint, A.-I. Dekkiche, A Generic Battery Model for the Dynamic Simulation of Hybrid Electric Vehicles, in: Vehicle Power and Propulsion Conference, 2007, pp. 284–289.

[15] C. M. Shepherd, Design of Primary and Secondary Cells II. An Equation Describing Battery Discharge, Journal of Electrochemical Society 112 (7) (1965) 657–664.

Appendix: Elements of the Matrix in Eq. (8)

$$\left.\begin{aligned}
G_{11} &= \frac{r_{\rm C}N_{\rm S} + R_{\rm L}(N_{\rm P}-1)}{\Delta}, \\
G_{12} &= \frac{\{r_{\rm C}N_{\rm S} + R_{\rm L}(N_{\rm P}-1)\}(N_{\rm S}-1)}{\Delta}, \\
G_{13} &= \frac{-R_{\rm L}N_{\rm S}(N_{\rm P}-1)}{\Delta}, \\
G_{21} &= \frac{-R_{\rm L}}{\Delta}, \\
G_{22} &= \frac{-R_{\rm L}(N_{\rm S}-1)}{\Delta}, \\
G_{23} &= \frac{\{R_{\rm L} + r_{\rm A} + r_{\rm B}(N_{\rm S}-1)\}N_{\rm S}}{\Delta}, \\
G_{31} &= \frac{r_{\rm C}N_{\rm S}}{\Delta}, \\
G_{32} &= \frac{r_{\rm C}N_{\rm S}(N_{\rm S}-1)}{\Delta}, \\
G_{33} &= \frac{\{r_{\rm A} + r_{\rm B}(N_{\rm S}-1)\}N_{\rm S}(N_{\rm P}-1)}{\Delta},
\end{aligned}\right\} \tag{14}$$

where

$$\Delta := \{-r_{\rm A} - r_{\rm B}(N_{\rm S}-1)\}\{-R_{\rm L}(N_{\rm P}-1) - r_{\rm C}N_{\rm S}\} + R_{\rm L}r_{\rm C}N_{\rm S}. \tag{15}$$

Table 1: Rated characteristics of two tested cylindrical cells.

	ICR18650	NCR18650
Nominal Capacity	2350 mAh	2900 mAh
Nominal Voltage	3.7 V	3.6 V
Cut-off Voltage	2.5 V	2.5 V

Table 2: Discharge capacities of two cells in series connection at ambient temperature of 28.3 °C. The symbol † denotes the value of discharge capacity under the single operation.

	Discharge Capacity / mAh
I1	2307 ($2326^{\dagger}$)
N1	2299 ($2839^{\dagger}$)
I1 + N1	2303

Table 3: Discharge capacities of two cells in parallel connection at ambient temperature of 28.5 °C.

	Discharge Capacity / mAh
I1	2301 ($2326^{\dagger}$)
N2	2833 ($2820^{\dagger}$)
I1 ‖ N1	5134

Table 4: Discharge capacities of four cells in series-parallel connection with cross coupling at ambient temperature of 28.6 °C.

	Discharge Capacity / mAh
I1	2306 ($2326^{\dagger}$)
N1	2563 ($2839^{\dagger}$)
N2	2817 ($2820^{\dagger}$)
N3	2556 ($2808^{\dagger}$)
Multicell Battery	5121

Table 5: Discharge capacities of four cells in series-parallel connection without cross coupling at ambient temperature of 29.1 °C.

	Discharge Capacity / mAh
I1	2314 (2326†)
N1	2303 (2839†)
N2	2702 (2820†)
N3	2698 (2808†)
Multicell Battery	5009

Table 6: Parameters of the circuit-based cell model for two cells used in this paper.

	ICR	NCR
E_0	2.7243 V	3.2124 V
K	0.0127 V	0.0148 V
Q_0	2.13 Ah	2.80 Ah
A	1.2006 V	0.9475 V
B	0.3838 Ah^{-1}	0.5135 Ah^{-1}
r	0.1097 Ω	0.0759 Ω

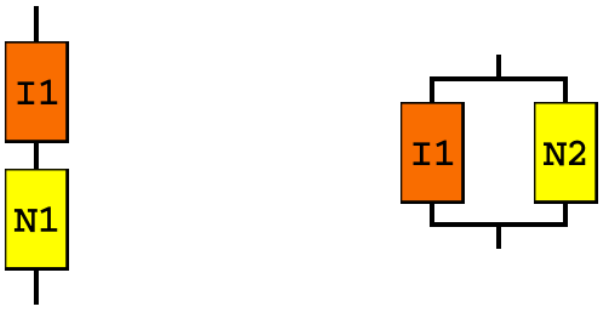

(a) series connection (b) parallel connection

Figure 1: Basic series and parallel connections of multicell battery with two different cells.

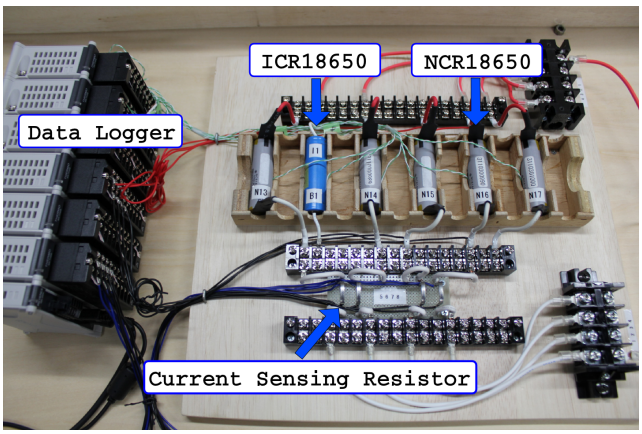

Figure 2: Experimental system of multicell lithium-ion battery.

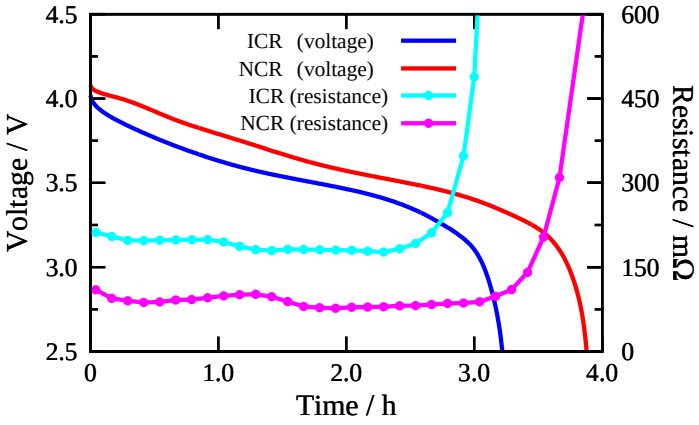

Figure 3: Discharge voltage and internal resistance of ICR and NCR at ambient temperature of 25.0 °C.

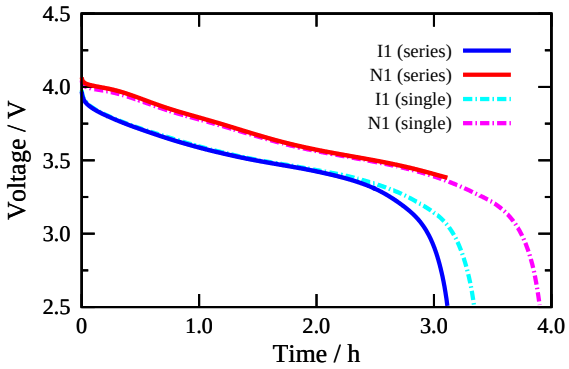

(a) discharge voltage

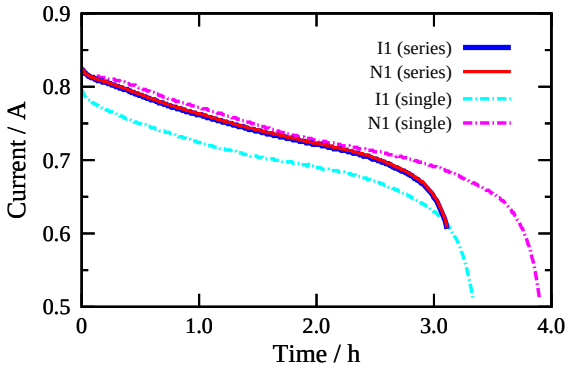

(b) discharge current

Figure 4: Discharge voltage and current of I1 and N1 in series connection at ambient temperature of 28.3 °C. The dashed lines show the discharge characteristics in the case of single operation.

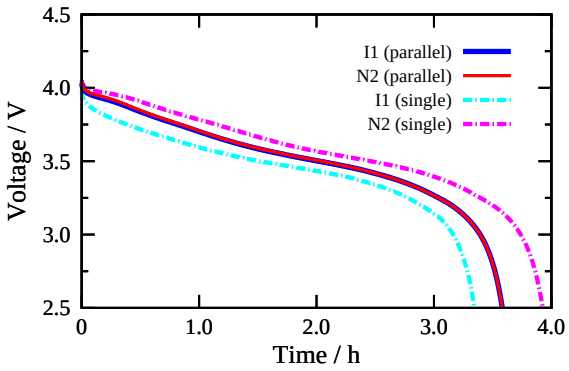

(a) discharge voltage

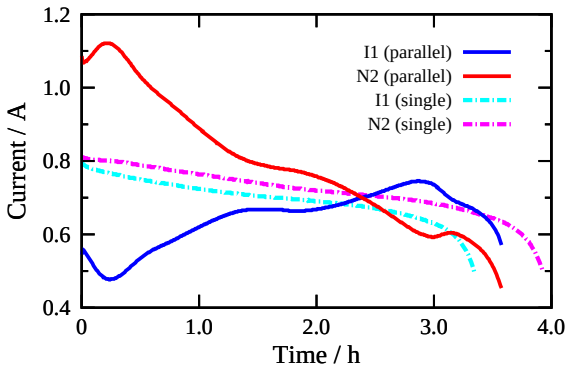

(b) discharge current

Figure 5: Discharge voltage and current of I1 and N2 in parallel connection at ambient temperature of 28.5 °C.

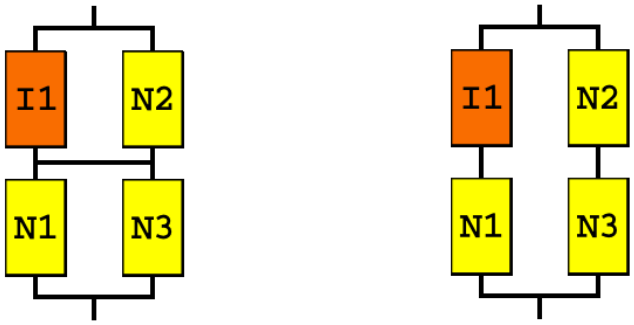

(a) with cross coupling (b) without cross coupling

Figure 6: Multicell battery of four cells in series-parallel connection.

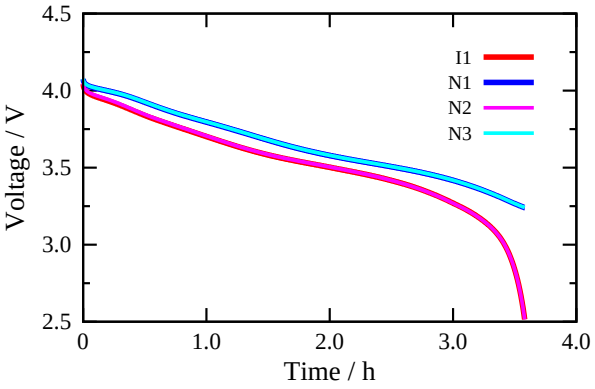

(a) discharge voltage

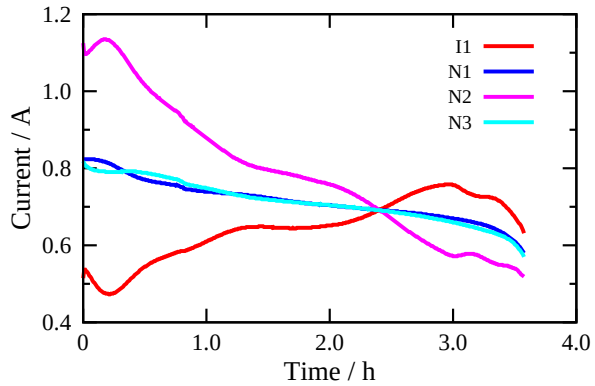

(b) discharge current

Figure 7: Discharge voltage and current of four cells in series-parallel connection with cross coupling at ambient temperature of 28.6 °C.

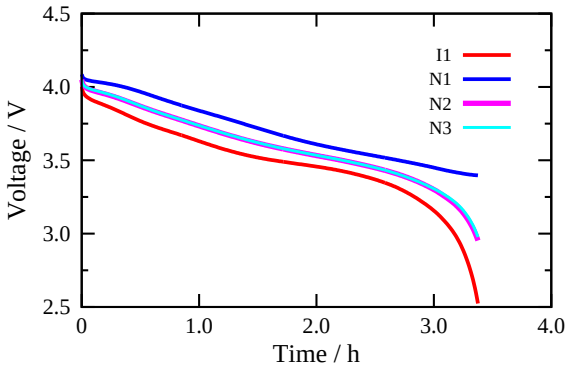

(a) discharge voltage

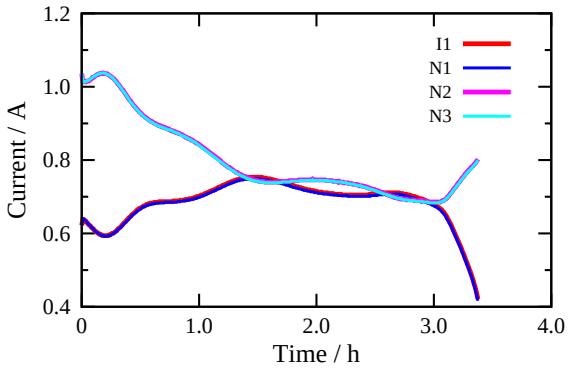

(b) discharge current

Figure 8: Discharge voltage and current of four cells in series-parallel connection without cross coupling at ambient temperature of 29.1 °C.

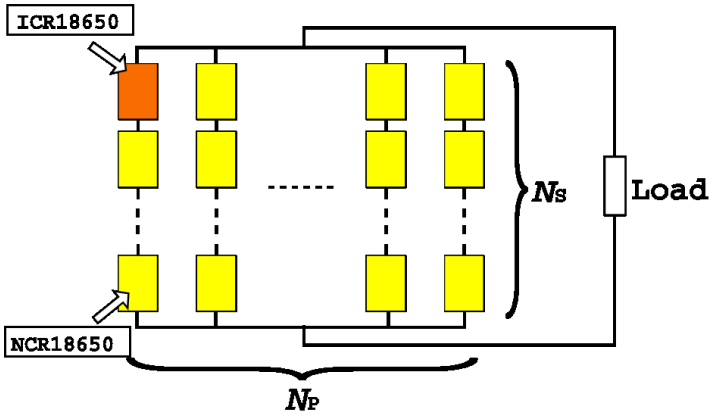

Figure 9: Configuration of multicell battery with nonuniform cells. The battery includes one ICR cell and many NCR cells.

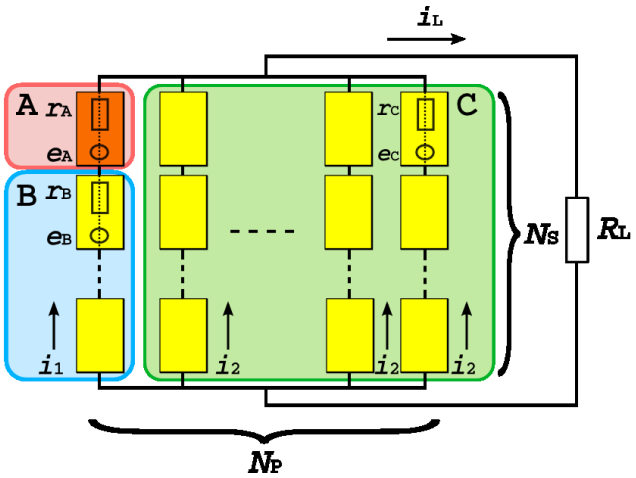

Figure 10: Classification of cells in the multicell battery. All of the cells are classified into A, B, and C according to the behavior of terminal voltage.

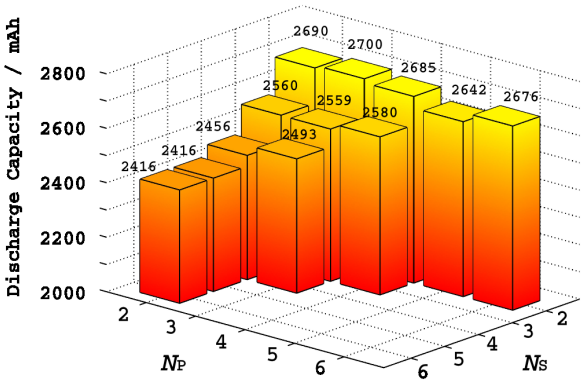

(a) experimental result

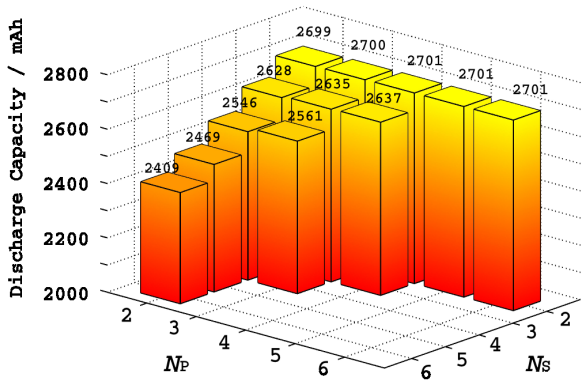

(b) simulation result

Figure 11: Discharge capacity Q for the multicell battery with $(N_{\mathrm{S}}, N_{\mathrm{P}})$ cells in the series-parallel connection.